Amyloidogenic Self-Assembly of Insulin Aggregates Probed by High Resolution Atomic Force Microscopy

Ralf Jansen,* Wojciech Dzwolak,† and Roland Winter*
*University of Dortmund, Department of Chemistry, Dortmund, Germany; and †High Pressure Research Center, Polish Academy of Sciences, Warsaw, Poland

ABSTRACT As the application of high-resolution atomic force microscopy (AFM) has led us recently to the discovery of a unique pressure-induced circular amyloid, we used the same approach to examine morphological events accompanying insulin aggregation under ambient conditions. This study presents the multistage, hierarchical character of the spontaneous fibrillation of insulin at low pH and at 60 and 70°C, and—due to the marked enhancement of image resolution achieved—brings new clues as to the fibrils' ultrastructure and mechanisms of its assembly. Specifically, focusing on the prefibrillar amorphous aggregates occurring 30 s after elevating temperature to the nucleation-enhancing 60°C, revealed the tendency of the globule-shaped oligomers to queue and assembly into elongated forms. This suggests that the shape of the nuclei itself predetermines—in part—the fibrillar architecture of the amyloid. Among first fibrillar features, short but relatively thick (8-nm) seedlike forms appeared on a very short timescale within the first minute of incubation. It has been shown that such fibrils are likely to act as lateral scaffolds for the growth of amyloid. By using phase-image AFM as a nanometer-resolved probe of viscoelastic surface properties, we were able to show that bundles of early protofilaments associated into parallel fibrils are capable of a cooperative transformation into twisted, highly ordered superhelices of the mature amyloid. Independently from producing evidence for the step-resolved character of the process, intermediate and morphologically heterogeneous forms were trapped and characterized, which yields direct evidence for the multipathway character of the amyloidogenesis of insulin. Apart from the faster kinetics, the increased temperature of 70°C leads to a higher degree of morphological variability: along straight rods, twisted ribbonlike structures, rod bundles, and ropelike structures become prominent in the corresponding AFM data.

INTRODUCTION

The growing body of evidence linking Alzheimer, Parkinson, or Creutzfeldt-Jakob diseases to protein misfolding and subsequent aggregation into the so-called amyloids (Harper et al., 1997; Sipe and Cohen, 2000; Jackson and Clarke, 2000; Serpell, 2000; Dobson, 2003; Rochet et al., 2004), has been drawing attention to amyloidogenic pathways and structures of non-native protein assemblies. The typical fibrillar morphology (Rochet and Lansbury, 2000) is, next to the β-cross x-ray diffraction patterns and characteristic tinctorial properties, one of the most prominent physicochemical hallmarks of amyloids. Recently, ideas as to the generic, polymeric character of amyloids (Fändrich and Dobson, 2002), and the importance of destabilization (or complete unfolding—e.g., Fändrich et al., 2003) of the native structure before protein aggregation have begun to emerge. However, the present understanding of the amyloid structure, and in particular, of the link between the protein backbone's β-conformation and its supramolecular packing, which invariably leads genetically and structurally unrelated proteins to perplexingly similar fibrillar morphologies, remains scattered. The majority of mature amyloids are unbranched fibrils (Rochet and Lansbury, 2000) consisting of several, often intertwined protofilaments (which may form an internal waterfilled canal—Perutz et al., 2002). Although amyloidal isolates either from in vivo samples or in vitro preparations are generally straight, some of them display more or less pronounced curvature (e.g., Bouchard et al., 2000). The range of accessible quaternary fibrillar folds is not yet limited to these structural motifs, as the study on apolipoprotein C-II, which forms closed rings of amyloid (Hatters et al., 2003), or our own recent work on pressure-induced circular insulin amyloid (Jansen et al., 2004), have shown. Such findings are of paramount importance for any generalized model of amyloid assembly, as they convey information about structural organization on a subfibrillar level. Specifically, the pressure-induced growth of the circular insulin amyloid suggests anisotropic packing within an ambient protofilament.

Formation of an amyloid reflects an alternative to the native packing conformational struggle of a polypeptide chain to 1), reduce its surface accessible area; 2), saturate hydrogen bonding; and 3), reach an alternative non-native global free energy minimum (Gazit, 2002). Therefore subsequent stages of hierarchical amyloid formation may be expected to enhance burial of hydrophobic residues and to promote energetically favorable hydrogen bonding. Untangling of amyloid architecture and intrafibrillar packing of the β-pleated sheets is the key issue in designing inhibitors of the fibrillar growth—pharmaceuticals that could prevent spreading of a misfolded protein in diseased tissues (Cohen and Kelly, 2003). Moreover, since subtle structural differences are thought to underlie the puzzling phenomenon of *prion*

Submitted July 1, 2004, and accepted for publication November 15, 2004.

Address reprint requests to Roland Winter, Tel.: 49-231-755-3900; Fax: 49-231-755-3901; E-mail: winter@pci.chemie.uni-dortmund.de.

0006-3495/05/02/1344/10 $2.00

doi: 10.1529/biophysj.104.048843

strains (Peretz et al., 2002; Tanaka et al., 2004), learning the mechanisms of assembly of amyloid fibrils may have a valuable contribution to the understanding of the etiology of the prion diseases. Yet, this is precisely the insoluble, uncrystallizable character of amyloids that severely limits the number of applicable structure-determining methods, such as nuclear magnetic resonance, or x-ray diffraction. One of the most potent research tools used for studying the structure of amyloids is atomic force microscopy (AFM). In particular, phase-shift-based AFM images, which can be recorded in tapping mode, may be more detailed and highlight areas with different elastic properties, and hence may yield new insight into the topology of growing insulin fibrils. This, as well as visualization of early unstructured aggregates, are the particularly advantageous features of AFM in studies on amyloidogenesis.

The physiological and therapeutic importance of insulin, e.g., the iatrogenic occurrence of insulin amyloid in tissues of diabetes I and II patients (Westermark et al., 1987), and the fact that insulin easily aggregates in vitro, have made the hormone an excellent model for protein aggregation studies (Nielsen et al., 2001a,b,c). Moreover, as the phenomenon of protein aggregation appears to reflect certain generic polymeric features of proteins (Fändrich and Dobson, 2002), studying mechanisms of protein aggregation on model systems is extremely useful for a better understanding of the molecular mechanisms of disease-associated amyloidogenesis. For instance, we have shown recently that, under certain conditions, the in vitro amyloidogenesis of insulin closely mimics certain aspects of the strain behavior of prion propagation (Dzwolak et al. 2004b).

Under physiological conditions, insulin is a hexamer, being able to bind two or four Zn^{2+} ions (e.g., Chang, et al., 1997). Decreasing pH and protein concentration shift the equilibrium toward smaller oligomers (Whittingham et al., 2002). The insulin monomer consists of two chains: a 21-residue-long A-chain and a 30-residue-long B-chain. The chains are connected by two disulfide bridges: A7–B7 and A20–B19, whereas a third bridge binds cysteine residues 6 and 11 of the A-chain (e.g., Chang, et al., 1997). The insulin aggregation involves only noncovalent interactions, and the disulfide bridges do not undergo recombination during the process. Therefore the conserved A6–A11 SS-bond is expected to cause a significant topological constraint and bending of the A-chain. The insulin aggregation is promoted under conditions favoring partly destabilized monomers and dimers, such as low pH, high temperature, and contact with hydrophobic media (e.g., Sluzky et al., 1991; Nielsen et al., 2001b). Several works implicated importance of particular amino acid residues for insulin aggregation; for example, the bovine insulin, diverging from the human protein at three amino acid positions (A8 Ala^{Bov}/Thr^{Hum}, A10 Val^{Bov}/Ile^{Hum}, and B30 Ala^{Bov}/Thr^{Hu}), aggregates more easily in vitro (Nielsen et al., 2001a). Studies on insulin derivatives established that the two B-chain's termini might play distinct roles in the amyloidogenesis: the C-terminal slows down the process, whereas the residues at the N-terminal are necessary for the lateral aggregation, i.e., enable protofilaments to form fibrils (Jimenez et al., 2002). Elsewhere it was shown that insulin fibrils' morphologies and the corresponding infrared spectra vary depending on conditions of their growth (Nielsen et al., 2001a,b,c; Whittingham et al., 2002; Dzwolak et al., 2004a). Insulin fibrils feature characteristics common to all amyloids: x-ray diffraction patterns; affinity to Congo Red and Thioflavin T; birefringence; biological dysfunction and high stability against temperature; pressure; low pH; and proteases. The infrared spectra of the amyloid suggest a parallel arrangement of the β-strands (Bouchard et al., 2000), and this remains in accordance with a three-dimensional model proposed for insulin amyloid fibrils (Jimenez et al., 2002). It appears that insulin aggregation must proceed through a bulky, non-native monomer (Ahmad et al., 2003), which quickly forms larger oligomers, as can be inferred from mass spectrometry (Nettleton et al., 2000). The existing morphological studies on insulin aggregation stress the hierarchical intertwisting of protofilaments (Jimenez et al., 2002; Khurana et al., 2003).

The rationale of this work was to inquire into the hierarchical assembly of the insulin amyloid and link the morphological transitions to conformational events observed by other biophysical and spectroscopic methods.

METHODS

Materials

Bovine insulin (from Sigma Aldrich, Steinheim, Germany) was used without further purification. Muscovite mica was purchased from Plano GmbH (Wetzlar, Germany). Other chemicals of *suprapur* or *ultrapure* grade were obtained from VWR (Merck GmbH, Darmstadt, Germany). Throughout all experiments, only ultrapure water (resistivity > 18 MΩ cm) was used. All accessories used for preparation and handling of insulin amyloid samples, such as vessels, tips, etc., were either disposable, single-packed, and classified as *biopur*, or—in the case of glass materials—cleaned with a saturated solution of sodium hydroxide in ethanol (both chemicals of the *suprapur* grade) for at least five days and subsequently rinsed with aqueous HCl-solution and ultrapure water.

Insulin amyloid formation

Fresh 0.1 wt % (0.17 mM) insulin solutions, pH-adjusted with diluted HCl at 1.6, were incubated at 60 or 70°C for 0 min, 0.5 min, 1 min, 5 min, 10 min, 20 min, 30 min, 1 h, 24 h, and 1 week. Immediately after the incubation, the protein samples were diluted 400 times with ultrapure hydrochloric acid in water (pH 1.6), and applied (30 μL) onto freshly-cleaved muscovite mica (9 mm diameter) attached to a 15-mm magnetic steel disc (serving as sample holder). The abrupt dilution of the samples immediately quenches the concentration-dependent aggregation process. Moreover, deposition of the tiny aqueous droplets on the mica surface is followed by very fast (timescale of seconds) evaporation of bulk solvent, which eventually prevents further aggregation. Therefore, throughout the following overnight dry incubation period no further structural transitions are likely to occur in the amyloid samples. The AFM-samples were dried gently with a nitrogen flow and left to dry overnight before the

measurements, which helps improve the quality of the AFM data. Control samples (freshly cleaved mica, mica, and aqueous HCl-solution) were also investigated with AFM to exclude possible artifacts.

AFM instrumentation

All AFM images were recorded on a MultiMode SPM microscope equipped with a Nanoscope IIIa Controller from Digital Instruments (Santa Barbara, CA). The microscope was coupled to an AS-12 E-scanner (13-μm) and an Extender Electronics Module EX-II (Digital Instruments, Santa Barbara, CA), which allows acquisition of phase images. Typically used AFM-probes respectively were Silicon SPM Sensors NCHR (force constant = 42 N/m; length = 125 μm; resonance frequency $\approx$300 kHz; nominal tip radius of curvature $\leq$5 nm) from Nanosensors (Neuchatel, Switzerland). For the high-resolution imaging, the AFM head (with optical block and base) was placed atop a commercially available active (piezo-actuated) vibrations-damping desk (from Halcyonics, Göttingen, Germany).

AFM operation and image analysis

Throughout the measurements, the *tapping-in-air* AFM mode was used. This affords both lateral and vertical resolution in a nanometric regime and enables nondestructive imaging of soft surfaces or weakly attached samples. Only completely dry samples were subjected to AFM-imaging. Because the tip approaching the surface induces a shift of AFM cantilevers' resonance frequency, the drive frequency, which has to be adjusted before engagement of the oscillating probe's first surface contact, is reduced until the vibrational amplitude reaches 95% of the maximum value. The typical value of drive-amplitude was 120–700 mV. To prevent thermal- or scanner-drifts, images were recorded after a warmup phase of at least 2 h.

Height and phase-shift data were respectively collected in the trace-retrace direction of a raster scan. Additionally, the scan-angle was changed in cases of repeated scans. To ensure correct height data, scanner calibration in the z direction was checked by height measurements on mica crystal layers, which exhibit precisely a step-depth of 1 nm. The scan rate was tuned proportionally to the area scanned (from 500 nm $\times$ 500 nm to 10 μm $\times$ 10 μm) and was kept within the 0.75–2 Hz range. To reduce the possibility of tip-contamination, samples were engaged at a zero scan position. The resolution of image acquisition was 512 pixels per line (512 $\times$ 512 pixels/image).

To minimize possible distortional effects, the lateral size determination method was applied. This permitted sufficiently accurate height determination (maximal vertical resolution was 0.1 Å). Horizontal distances were only ascertained if height data between two corresponding topographic maxima could be unambiguously determined. Vertical dimensions of the fibrillar aggregates were obtained from individual cross-section profiles generated by the AFM's accessory data analysis software. Whenever the size of a probed object permitted, 20 subsequent measurements of an individual feature were carried out and averaged. If necessary, only first-order plane-fittings were performed with the analytical software. If a small substrate tilt angle remained, the height was measured twice, at both the *cis*- and *trans*-positions. Fibril periodicity was determined by two methods after profiling the longitudinal fibril axis: 1), through the averaging of distances between two neighboring maxima; and 2), through the averaging of distances between the remotest maxima divided by the number of elevations. Only if the two sets of data showed accordance (occasionally an exact location of the apex is difficult), is the data further discussed.

RESULTS AND DISCUSSION

Prefibrillar stage

Fig. 1 presents the progress of the spontaneous amyloidogenesis of insulin at 60° (*left panel*) and 70°C (*right panel*)

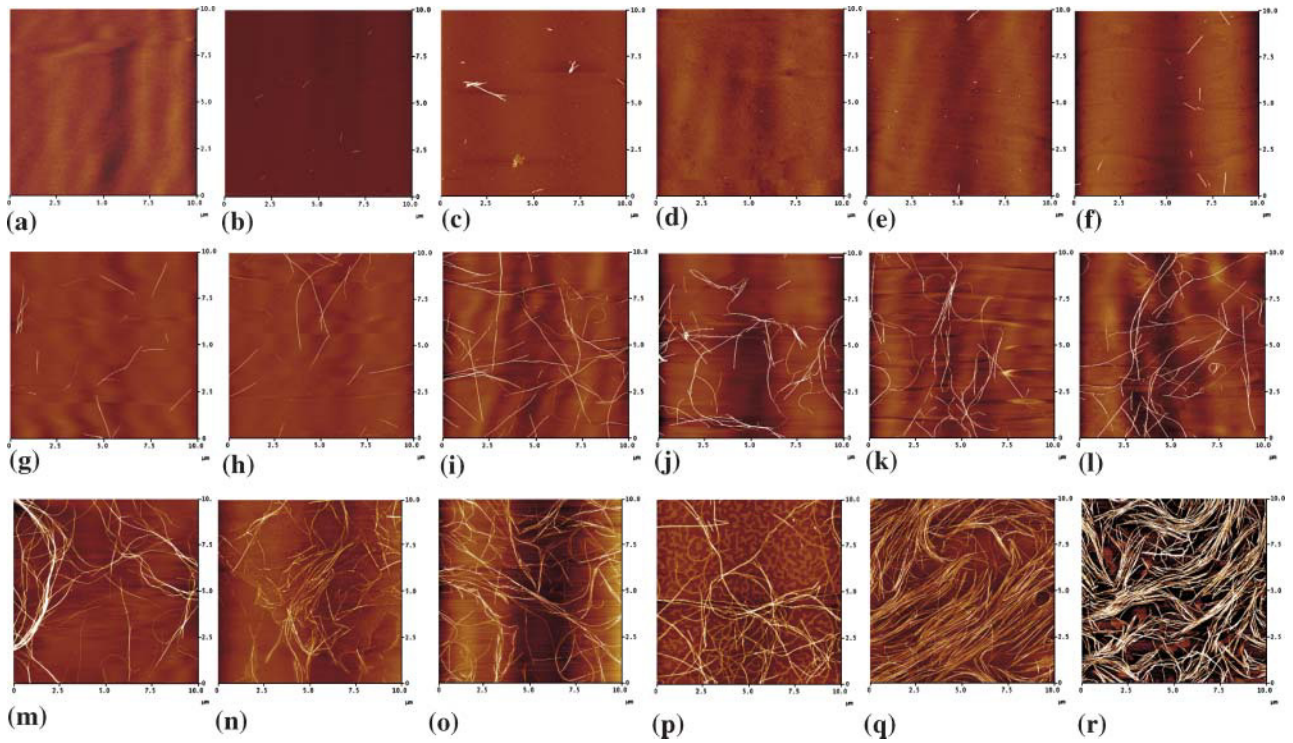

FIGURE 1 The overview of insulin fibrillization at 60° (*left*) and 70°C (*right*) monitored by time-lapse AFM. The following images correspond to: 0 min (a, j), 1 min (b, k), 5 min (c, l), 10 min (d, m), 20 min (e, n), 30 min (f, o), 1 h (g, p), 1 day (h, q), and 1 week (i, r). The scan size of each picture is 10 μm $\times$ 10 μm.

monitored by time-lapse AFM. The increased temperature shortens the lag phase of the aggregation, which is defined as lapse-time passed until the appearance of first fibrillar forms (rather than of transient early amorphous aggregates—see Fig. 1, *b*, *c*, and *j*). The lag phase of insulin aggregation may be monitored by a number of techniques sensitive to larger protein assemblies (e.g., light scattering) or selectively detecting the amyloid fibrils (fluorescence of amyloids labeled with thioflavin T; e.g., Jansen et al., 2004). Unless the aggregation process is enhanced by preformed insulin amyloid (the so-called seeding—Dzwolak et al., 2004b), lag phase is a typical feature of protein amyloidogenesis corresponding to the thermodynamically unfavorable nucleation process (Bouchard et al., 2000; Nielsen et al., 2001b). The tiniest seedlike forms appear within the first minute of incubation at either temperature. Once a sufficient amount of nuclei is formed, the following phase of fibrils' elongation becomes the major route of the conformational transition of insulin. This is reflected by the rapid increase in number of fibrils and the increasing complexity of fibrillar topology (Fig. 1, *e–i*, and *m–r*). Some characteristic traits of the mature amyloid fibrils are the tendencies to bend, twist, and agglomerate. At 60°C, primary branches and twists occur after 10 min, and are followed by bent structures. The lateral association is seen in the corresponding AFM images after 30 min at 60°C, but already after ~20 min at 70°C. The further growth beyond 1 h is accompanied by formation of superfibrillar structures. The increased temperature also appears to accelerate the elongation stage. Unlike at 60°C, the fibrillization at 70°C appears to be complete within ~24 h (Fig. 1 *q*) and no more oligomers are detected. The AFM images of the mature amyloid at 70°C (Fig. 1, *q* and *r*) clearly show domains of parallel fibrils with little tendency to criss-cross.

After this brief characterization of the gross stages of insulin amyloidogenesis, a more detailed analysis will be put forward. Fig. 2 shows the unheated insulin sample, which at room temperature (20°C) has little tendency to aggregate. The two images present singular particles randomly distributed over the whole surface. The particles have heights of 1.1 ± 0.2 nm. Given the accuracy of the height determination and the x-ray diffraction and small-angle x-ray scattering data (e.g., Nielsen et al., 2001b; Ahmad et al., 2003) on the actual dimensions of native insulin monomers (1.11 nm) and dimers (1.49 nm)—the two predominant species at this low pH—the particles appear to be lying flat on the mica surface.

The shortest incubation at 60°C (or 70°C) applied to insulin samples was only 30 s; yet as Fig. 3 *a* proves, this treatment is capable of already inducing pronounced changes in morphology of the small insulin particles, which immediately begin to cluster. Previous studies have pointed out that—at low pH and in the absence of co-solvents—the dimeric insulin must undergo temperature-induced monomerization before the actual aggregation (Nettleton et al., 2000; Hua and Weiss, 2004). As we determined earlier, this preliminary stage of the aggregation process is endothermic (Dzwolak et al., 2003) and occurs above 50°C. The monomers are prone to fast oligomerization. Although newly-formed oligomers initially retain nativelike structure (Bouchard et al., 2000), they are the last pre-amyloidal state with a native secondary fold. The once-formed oligomers will remain after the temperature decrease, acting as early nucleation centers. Interestingly, the clusters are not spherical, and pearl-like arrangements and elongated forms appear to dominate (examples are marked in Fig. 3 *a* with *arrows* and a *green line*). Given the height scaling used in these measurements, the elongated species are not loosely interacting groups of single particles, but, instead, unified entities. The brief high temperature treatment of insulin results in a marked broadening of the height-distribution of the particles and its shift toward larger oligomers, which is shown in Fig. 3 *b*. Such large (3.2–3.9 nm in diameter) partially unfolded spherical oligomers are apparently capable of merging into the amyloid precursor. The remarkable size may result from both the number of monomers involved, and the fact that insulin aggregation intermediates are rather bulky and swollen with water (Dzwolak et al., 2003; Ahmad et al., 2003).

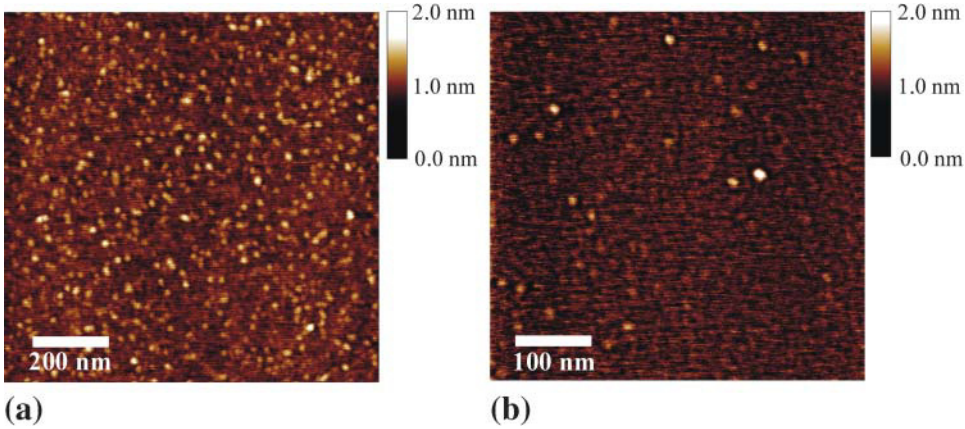

FIGURE 2 An AFM height image of fresh, unheated insulin solution, pH 1.6, $T = 20$°C (*a*). The magnified image in *b* shows spherical shapes of the protein particles.

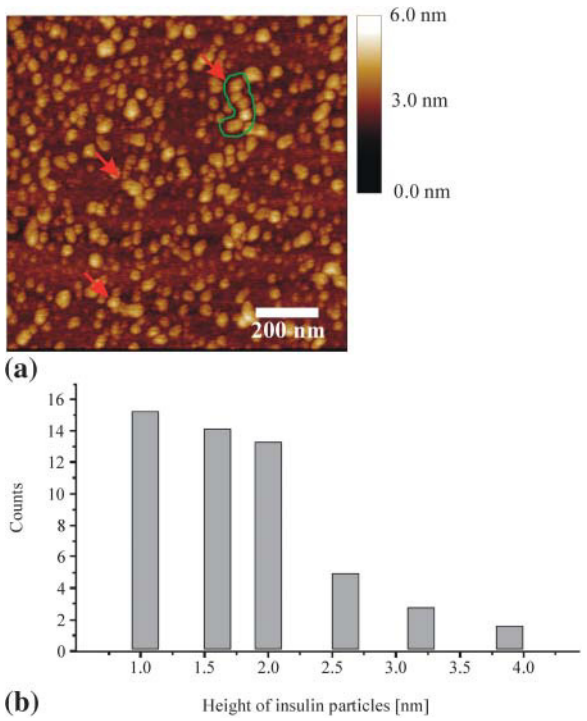

FIGURE 3 (*a*) AFM height image of the early insulin aggregates formed during the first 30 s of incubation at 60°C; the arrows mark the elongated, prefibrillar loose aggregates. Averaged size-distribution of the particles (*b*).

It is a well-established experimental fact that, upon insulin fibrillogenesis, the first to appear are thin forms ~1.2 ± 0.3-nm in diameter, with elongated features (Khurana et al., 2003), which are likely to consist of tubularly-stacked infinite β-helices (Jimenez et al., 2002). Such protofilaments merge and intertwist, yielding thin fibrils, which are capable of further association and twining, producing mature amyloid. The driving force transforming destabilized protein molecules to protofibrils, and protofilaments to fibrils, arises from hydrophobic and electrostatic interactions. The same type of interactions play a role in the lateral clumping of monomers/oligomers and fibrils. The compact mature fibrillar structures formed at the endpoint of the aggregation process may hence result from an effort to minimize the exposure of hydrophobic residues.

Such a hierarchical scenario of amyloidogenesis (Aggeli et al., 2001) has been observed for several proteins including β_2-microglobulin (Kad et al., 2003), α-synuclein (Khurana et al., 2003), yeast prion protein Ure2 (Jiang et al., 2004), and insulin (Bouchard et al., 2000; Jimenez et al., 2002; Khurana et al., 2003). In this study, however, we have also observed, along the typical transient structural motifs, that lateral interactions normally dominating at the later stages of fibrillogenesis and responsible for the thickening of the fibers may, in fact, play a role at the very beginning of the process—and lead to an alternative subpathway of amyloid assembly.

Early fibrillar forms

Among the first fibrillar forms of insulin aggregates appearing within the first 60 s of the incubation at 60°C, few and relatively thick rodlike specimens can be seen, which will be abundant at a later stage of the aggregation process (after ~5 min). An example shown in Fig. 4 consists of four cordlike subunits. The AFM image of the fibroid of the total length of 544 ± 12 nm may be interpreted as either a periodically twisted structure with a regular helical thread of 52 ± 2 nm, or linearly-staggered elements, each 52 ± 2 nm long, constituting a longer topological block. On average, these fibrils are ~80–500 nm long, and rather uniformly 4.4 ± 0.3 nm high (the average estimation is based on 20 measurements), which otherwise corresponds to the thickness of regular mature insulin amyloid (Khurana et al., 2003). The 70°C preparations yield populations of equally long, but 2.9 ± 0.6-nm or 6.5 ± 0.6-nm high, seeds. In Fig. 4 *a*, the helical groove-depth is 1.7 ± 0.14 nm. The height values corresponding to the three outer subcords seen in Fig. 4 *a* are 7.2 ± 0.29 nm (*left*), 7.9 ± 0.37 nm (*central*), and 5.3 ± 0.25 nm (*right*).

A thorough examination of these initial forms is of interest, as in this early timescale of the aggregation process both the nucleation and elongation coexist, and may influence each other. Interestingly, a closer scrutiny of the insulin aggregates obtained after 1-min incubation at 60°C indicates that clusters of swollen insulin particles tend to align within the immediate vicinity of the early fibers (Fig. 4, *b*, *d*, and *e*). This suggests that the once-formed fibroid enhances—through lateral interactions—formation of subsequent fibers. When attempting to elucidate a plausible mechanism of formation of these early, yet relatively thick fibrils, it must be taken into account that the fibrils' ends are not frayed, i.e., the ingredient subcords are of equal length and are evenly aligned. Such an effect would be quite improbable and surprising, should the fiber be produced by a spontaneous association of several free pre-existing protofilaments of the same length. On the contrary, it seems that a single protofilament may act as a lateral template or scaffold for small insulin particles, which would constitute a neighboring subcordlike features in the fibril shown in Fig. 4 *a*. This *protofilament + monomers/oligomers* scenario is an alternative pathway to the otherwise dominating *protofilament + protofilament* way of the protein fibrils' lateral growth.

In Fig. 5 *a*, height and in Fig. 5 *b*, phase AFM images of the morphological features obtained after 5 min of the 60°C incubation are shown. The fibers are considerably thicker (the average diameter judged from the height data is 9.3 ± 0.7 nm), and their surface appears to be structured with 6–8 subcords aligned in parallel, which are likely to be protofilaments of an individual height of ~2.0 ± 0.5 nm. Therefore, depending on internal packing, it could be approximately estimated that the thick fiber may consist of over a dozen of laterally associated protofilaments.

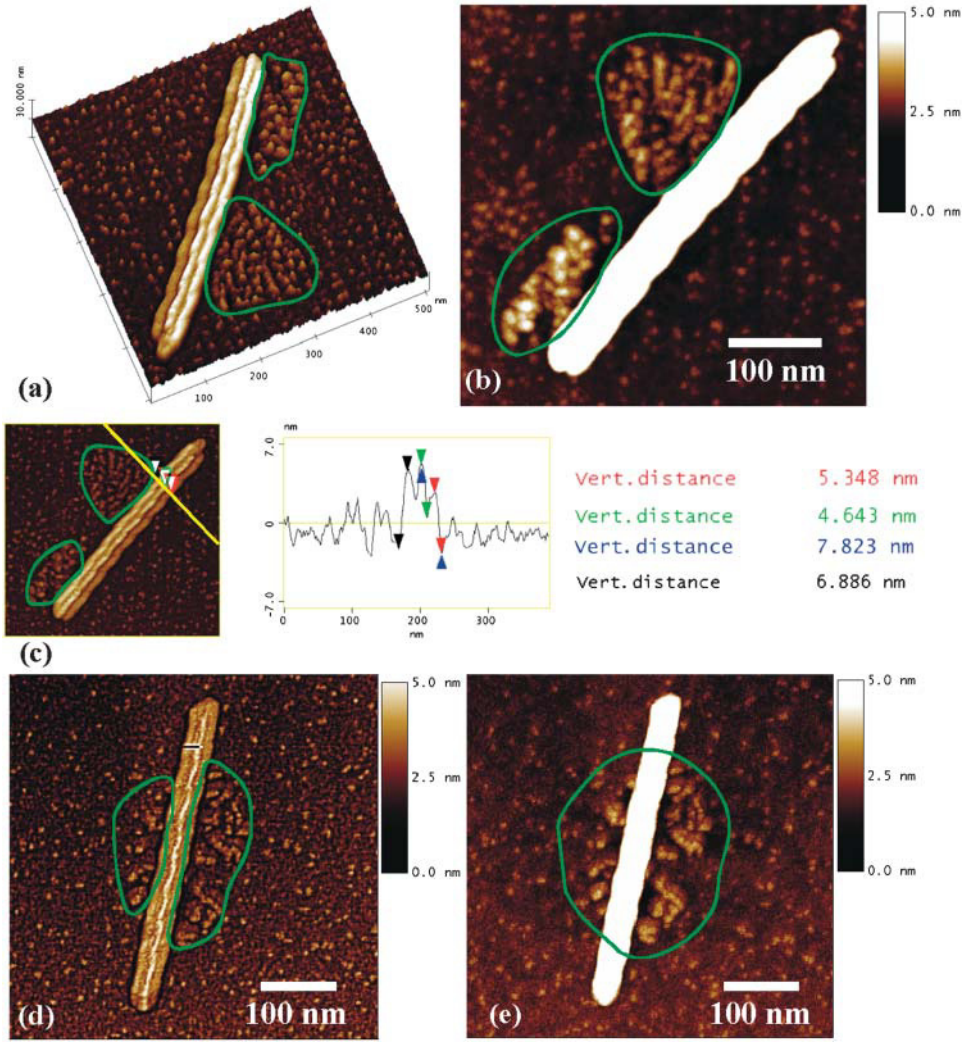

FIGURE 4 First rodlike insulin aggregates formed after 1 min at 60°C (*a* and *b*). An example of the measurement of filament height (*c*). Particles of prefibrillar aggregates tend to cluster in the proximity of the early fibers (*b*, *d*, and *e*)—marked in green line.

Phase AFM (Fig. 5 *b*) enables our probing the relative hardness of the imaged object. This approach has been employed here to deconvolute the fibrillar structure shown in Fig. 5 *a* into ingredient subcords of various packing, four or six of which are apparently distinguishable on a single's fiber's surface. Although it is known that parts of the insulin chains, such as the C-terminal of the B-chain, are not expected to participate in the tight intra- and interfibrillar packing (therefore giving rise to loose and soft elements protruding alongside the protofilament—Jimenez et al.,

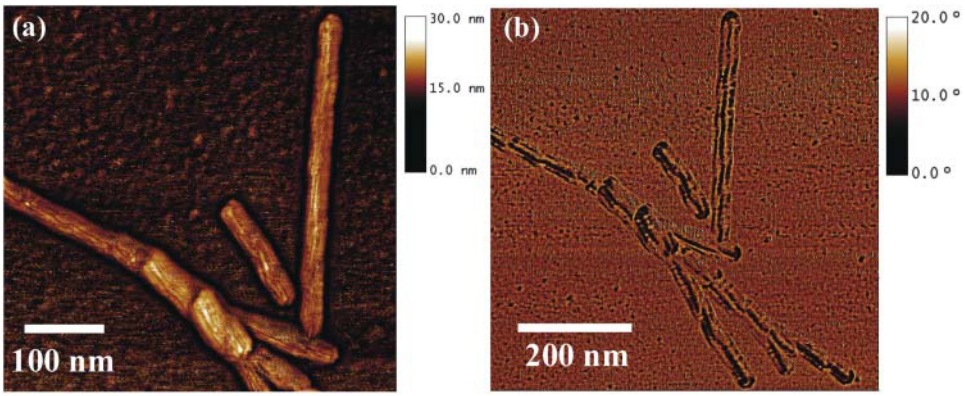

FIGURE 5 Height (*a*) and phase-shift (*b*) AFM images of a cluster of insulin aggregates formed after 5 min incubation at 60°C.

2002), it may be as well the different degrees of packing of protofilaments in the fibers' core and on its surface that evoke this effect.

The prolonged 10-min incubation at 60°C promotes further elongation of the fibers even up to 2.8 μm. The fibrils grown at 70°C on the same timescale are longer (up to 5.5 μm) and approximately three times more abundant (25 particles at 60°C versus 71 at 70°C particles per surface unit). Apart from the faster kinetics, the increased temperature leads to a more complex morphological variability: long straight rods, twisted ribbonlike structures, rod bundles, and ropelike structures become prominent in the corresponding AFM data. Highly twisted fibrils, along with the species of negligible helicity, have been reported earlier for different insulin amyloid preparations (Nielsen et al., 2001c). Fig. 6 *a* shows a representative example of the morphological variability in insulin fibrillar aggregates grown for 10 min at 70°C. The features can be classified as: *parallel tubular fibers*, *twisted ribbonlike structures*, *rod bundles*, and *ropelike textures*. The seven distinguishable fibers seen in

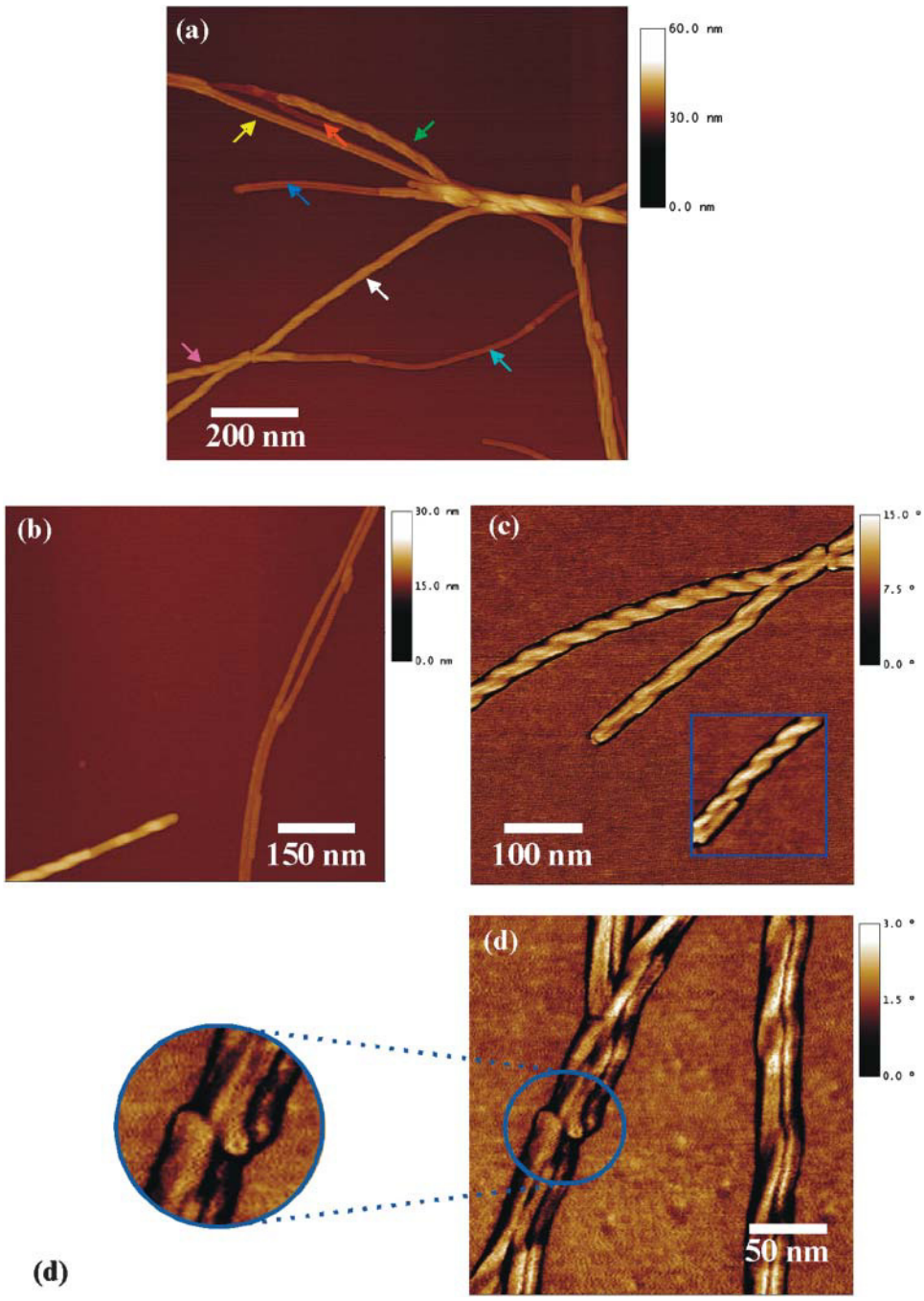

FIGURE 6 Morphological variability in insulin amyloid samples obtained after 10-min incubation at 70°C (*a–c*). Fibrils diameters: 4.2 ± 0.20 nm (*red*), 5.5 ± 0.57 nm (*turquoise*), 7.2 ± 0.50 nm (*blue*), and 9.0 ± 0.36 nm (*yellow*). Image of fibers obtained through 10-min incubation of native insulin at 60°C (*d*).

this picture were inspected in a detailed manner: four of them are tubular or ribbonlike double-corded (indicated by the *red, blue, yellow* and *turquoise arrows*) and three others are more or less twisted (marked with the *green, white* and *pink arrows*).

Another difference between the 10-min insulin aggregate preparations at 60 and 70°C concerns diversely convoluted shapes, whose presence is more pronounced in the latter case. These forms vary from slight bends over double turns to semicircles of variable radii of curvature (not smaller than 250 nm). In the 70°C samples, semicircles and sinusoidal bends are observed. We showed earlier that the pressure-induced circular amyloid of insulin consists of several loops of a thin and untwisting form, possibly a single protofilament (Jansen et al., 2004). It may be therefore hypothesized that the protofilament structure gives rise to an inherent mechanical strain, which may be relaxed either by a collective twisting of associated protofilaments, or curling them. The observed tendency of untwisted lateral agglomerates (Fig. 5) to transform cooperatively into hierarchically twisted features (Fig. 6) may be a consequence of a more effective relaxation of the mechanical strain (at a similar entropic cost of the assembly).

Structural polymorphism of mature fibrils

Fig. 6, *b* and *c*, represents other morphological motifs commonly found in the insulin aggregate 10-min preparations at 70°C; for example, two laterally connected double-strand fibers of equal height of 3.1 nm (Fig. 6 *b*) splitting over a certain distance, or, visible in Fig. 6 *c*, two highly-twisted fibrils with different morphologies overlapping each other. It appears therefore that even for a homogenous insulin sample undergoing uniform temperature treatment, there is still more than one mode of superhelical assembly of protofilaments. In Fig. 6 *d*, the end of one thread (indicated by the *blue circle*) seems to grow out of the image's plane facing vertically upwards and making the subfibrils interior penetrable to the AFM tip. The zoom-in reveals the entrance to a fibrillar canal of ~1-nm diameter. This, in fact, is direct evidence supporting the model of amyloids as waterfilled nanotubes (Perutz et al., 2002).

The juxtaposed differences between the populations of fibers grown at 60 and 70°C clearly concern not only the rate of the aggregation process, but different quaternary folds as well. Although different distribution profiles of fibrillar features may still be explained in terms of kinetic effects (temperature may differently affect the kinetics at various stages of the assembly, effectively marginalizing certain sequential processes), the higher temperature may also have a more direct effect on amyloidogenesis, for instance by increasing the thermal energy of the interacting molecules and hence causing the alignment of protofilaments to become less accurate. Such unspecific effects may contribute to morphological differences in any protein's amyloid samples induced at high temperature. However, the herein-observed morphological variation after increasing temperature bears a more profound meaning in light of the ongoing debate as to the identity of the protein's aggregation-prone conformation (completely unfolded, or partly unfolded protein) and our own study, showing that under similar conditions, bovine insulin is substantially more unfolded at 70 than at 60°C (Dzwolak et al., 2003). According to the polymeric paradigm (Fändrich and Dobson, 2002) of amyloidogenesis and the therein-implicated importance of backbone interactions, the more the native structure becomes distorted (and the protein backbone becomes exposed), the higher the chance that the protein steps onto the amyloidogenic pathway. Although considerable evidence suggests that only partial destabilization of insulin is the prerequisite for its aggregation (Ahmad et al., 2003), the herein-presented data points out that additional temperature-induced destabilization may be a factor broadening the range of accessible fibrillar forms.

An interesting aspect of the late stages of the amyloidogenic assembly is provided by AFM data on insulin samples heated at 70°C for 20 (Fig. 7 *a*) and 30 (Fig. 7 *b*) min. The two fibers marked with the green and blue arrows are of the comparable height of 6.5 ± 0.5 nm, and appears to consist of joined segments ~153 ± 8 nm long. The fiber's height at intersegment joints is only 3.4 ± 0.2 nm. In the vicinity of

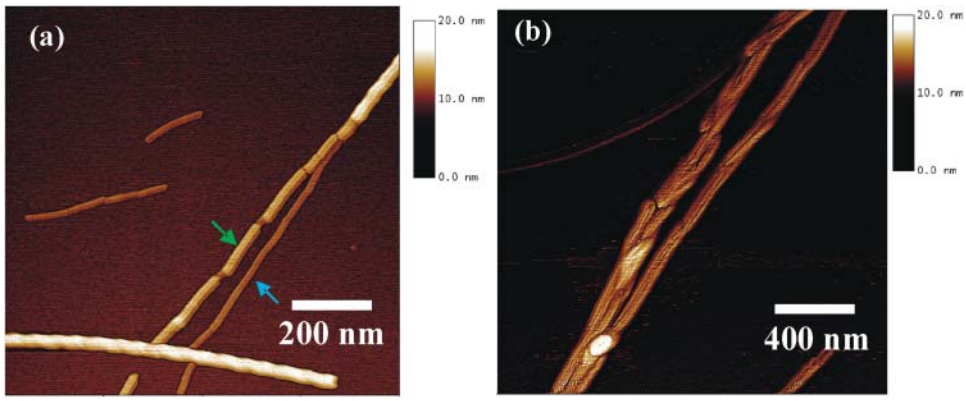

FIGURE 7 AFM images of mature insulin amyloids grown at 70°C after a 2-min (*a*) or 30-min (*b*) incubation.

the fibers of such chained appearance, there are single amyloid stretches of 155 ± 5 nm length, which is an excellent match with the chain unit's size. Another interesting object visible in Fig. 7 *a* is a pair of such units. This data may be interpreted as yet another way of assembling amyloid fibrils through chainlike queuing of preformed discrete amyloid subunits.

Under these experimental conditions, no prominent qualitative changes in the elementary morphological folds were observed at times of incubation exceeding 1 h. The full fibril length is not definable any longer for dimensions exceeding the maximum (16 μm) scan size of the apparatus. In general, the lateral binding seems to be highly variable. A new aspect is the formation of so-called *superfibrillar* aggregates as shown in Fig. 1 *g*: 5 (often also 10–15 or sometimes even >20) fibers with diverse characteristics (like tubular, twisted, or undulated forms) and diameters generate both tight- and loose-plait ropelike forms (diameter: 5–25 nm) with endings fraying in single fibers.

In contrast to the 60°C incubation, in which a fibril concentration increase of ~1:4 (235 fibers versus 325 fibers) can be determined in the time period between 1 day and 1 week, a noteworthy fibril concentration change at 70°C in the same period does not take place. This suggests that the aggregation process is essentially completed after 1 h at 70°C. Interestingly, in these two samples (1 h and 1 week incubation at 70°C) the fibers do not criss-cross. In fact there are large meanderlike areas, wherein fibrils are uniformly oriented. This supports the proposed mechanism of the early fibrils shown in Fig. 4 acting as lateral scaffolds for formation of following fibrils, which at the same time ensures ordered, parallel organization of large domains of fibrils.

Studies on the pathogenic amyloidogenic self-assembly of proteins are showing that different transient morphological forms of aggregates have varying neurotoxicity levels (e.g., neurotoxic protofibrils of α-synuclein—Rochet et al., 2004). On the other hand, seeding experiments suggest that mature, solid fibrils act as the most effective catalysts of amyloidogenesis in vitro (Harper et al., 1997; Dzwolak et al., 2004b). The herein-reported multiple pathways of insulin amyloidogenesis and the resulting heterogeneity of the mature amyloid illustrate the kinetically controlled character of the process. That the short protofilaments and fibrils act as lateral scaffolds for further aggregation shows that preventing elongation of amyloid through the terminal docking mechanism may not be a sufficient therapeutic strategy of eliminating neurotoxicity in vivo.

In conclusion, we have shown that insulin amyloidogenesis in vitro induced by the en masse destabilization of native dimers proceeds through a multipathway assembling scheme, which employs—on the one hand—the hierarchical intertwisting reported earlier; and on the other hand, employs lateral interactions of single particles and fibrils, leading to larger domains of features aligned in parallel (Fig. 8). Such an alternative scenario of fibrillar self-assembly may, in the end, lead to morphologies with a screwlike outlook, otherwise postulated to result from the hierarchical twisting. The herein-discussed polymorphism of insulin amyloids, and the putative lateral assembling interactions between the seedlike forms and early nativelike molecules, are important—since both appear to correspond to in vivo cases of amyloid proliferation, and may contribute to a deeper understanding of the amyloidal-type of neurotoxicity, as well as the intra- and extracellular mechanisms of the propagation of amyloids.

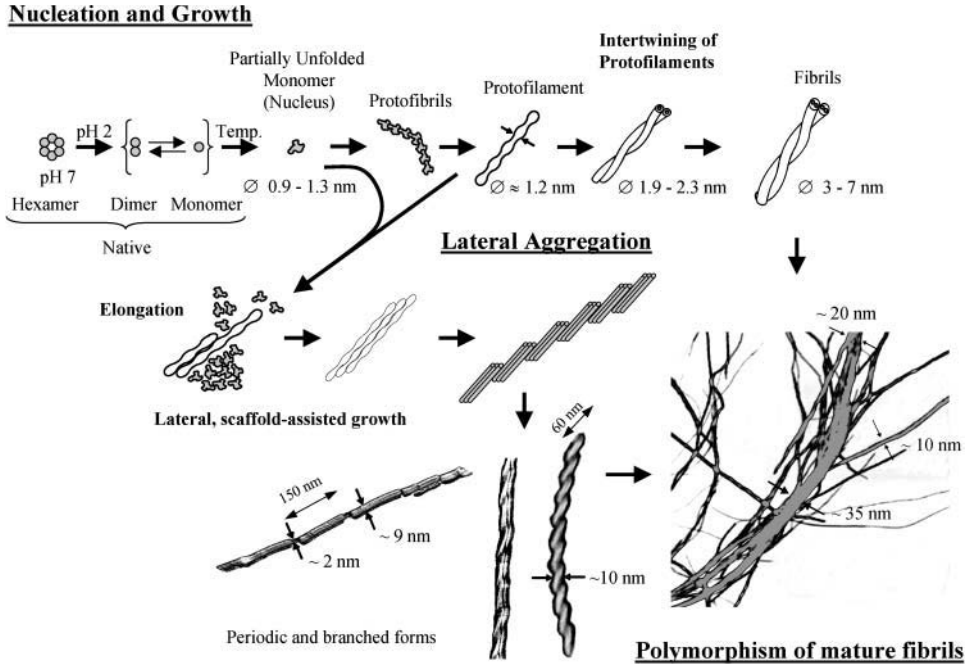

FIGURE 8 Generalized scheme of the multipathway fibrillization of insulin. The lateral interaction of early, prefibrillar forms with protofibrils and protofilaments, followed by the lateral association of protofilaments, is a self-assembly route alternative to the hierarchical intertwining of protofilaments. The observed polymorphism of mature amyloid samples suggests that, under the given conditions, insulin fibrillization proceeds from both pathways.

Financial support from the Deutsche Forschungsgemeinschaft and the Fonds der Chemischen Industrie and the COST D30 action ''High Pressure Tuning of Biochemical Processes: Protein Dynamics and Aggregation'' is gratefully acknowledged.

REFERENCES

Aggeli, A., I. A. Nyrkova, M. Bell, R. Harding, L. Carrick, T. C. McLeish, A. N. Semenov, and N. Boden. 2001. Hierarchical self-assembly of chiral rod-like molecules as a model for peptide β-sheet tapes, ribbons, fibrils, and fibers. *Proc. Natl. Acad. Sci. USA*. 98:11857–11862.

Ahmad, A., I. S. Millett, S. Doniach, V. N. Uversky, and A. L. Fink. 2003. Partially folded intermediates in insulin fibrillation. *Biochemistry*. 42: 11404–11416.

Bouchard, M., J. Zurdo, E. J. Nettleton, C. M. Dobson, and C. V. Robinson. 2000. Formation of insulin amyloid fibrils followed by FTIR simultaneously with CD and electron microscopy. *Protein Sci*. 9:1960–1967.

Chang, X., A. M. Jorgensen, P. Bardrum, and J. J. Led. 1997. Solution structures of the R6 human insulin hexamer. *Biochemistry*. 36:9409–9422.

Cohen, F. E., and J. W. Kelly. 2003. Therapeutic approaches to protein-misfolding diseases. *Nature*. 426:905–909.

Dobson, C. M. 2003. Protein folding and misfolding. *Nature*. 426:884–890.

Dzwolak, W., R. Ravindra, J. Lendermann, and R. Winter. 2003. Aggregation of bovine insulin probed by DSC/PPC calorimetry and FTIR spectroscopy. *Biochemistry*. 42:11347–11355.

Dzwolak, W., R. Ravindra, and R. Winter. 2004a. Hydration and structure—the two sides of the insulin aggregation process. *Phys. Chem. Chem. Phys*. 6:1938–1943.

Dzwolak, W., V. Smirnovas, R. Jansen, and R. Winter. 2004b. Insulin forms amyloid in a strain-dependent manner: an FT-IR spectroscopic study. *Protein Sci*. 13:1927–1932.

Fändrich, M., and C. M. Dobson. 2002. The behaviour of polyamino acids reveals an inverse side chain effect in amyloid structure formation. *EMBO J*. 21:5682–5690.

Fändrich, M., V. Forge, K. Buder, M. Kittler, C. M. Dobson, and S. Diekmann. 2003. Myoglobin forms amyloid fibrils by association of unfolded polypeptide segments. *Proc. Natl. Acad. Sci. USA*. 100:15463–15468.

Gazit, E. 2002. The ''correctly folded'' state of proteins: is it a metastable state? *Angew. Chem. Int. Ed. Engl*. 41:257–259.

Harper, J. D., C. M. Lieber, and P. T. Jr. Lansbury. 1997. Atomic force microscopic imaging of seeded fibril formation and fibril branching by the Alzheimer's disease amyloid-β protein. *Chem. Biol*. 4:951–959.

Hatters, D. M., C. A. MacRaild, R. Daniels, W. S. Gosal, N. H. Thomson, J. A. Jones, J. J. Davis, C. E. MacPhee, C. M. Dobson, and G. J. Howlett. 2003. The circularization of amyloid fibrils formed by apolipoprotein C–II. *Biophys. J*. 85:3979–3990.

Hua, Q. X., and M. A. Weiss. 2004. Mechanism of insulin fibrillation: the structure of insulin under amyloidogenic conditions resembles a protein-folding intermediate. *J. Biol. Chem*. 279:21449–21460.

Jackson, G. S., and A. R. Clarke. 2000. Mammalian prion proteins. *Curr. Opin. Struct. Biol*. 10:69–74.

Jansen, R., S. Grudzielanek, W. Dzwolak, and R. Winter. 2004. High pressure promotes circularly shaped insulin amyloid. *J. Mol. Biol*. 338: 203–206.

Jiang, Y., H. Li, L. Zhu, J. M. Zhou, and S. Perrett. 2004. Amyloid nucleation and hierarchical assembly of Ure2p fibrils. Role of asparagine/glutamine repeat and nonrepeat regions of the prion domains. *J. Biol. Chem*. 279:3361–3369.

Jimenez, J. L., E. J. Nettleton, M. Bouchard, C. V. Robinson, C. M. Dobson, and H. R. Saibil. 2002. The protofilament structure of insulin amyloid fibrils. *Proc. Natl. Acad. Sci. USA*. 99:9196–9201.

Kad, N. M., S. L. Myers, D. P. Smith, D. A. Smith, S. E. Radford, and N. H. Thomson. 2003. Hierarchical assembly of β2-microglobulin amyloid in vitro revealed by atomic force microscopy. *J. Mol. Biol*. 330:785–797.

Khurana, R., C. Ionescu-Zanetti, M. Pope, J. Li, L. Nielson, M. Ramirez-Alvarado, L. Regan, A. L. Fink, and C. A. Carter. 2003. A general model for amyloid fibril assembly based on morphological studies using atomic force microscopy. *Biophys. J*. 85:1135–1144.

Nielsen, L., S. Frokjaer, J. Brange, V. N. Uversky, and A. L. Fink. 2001a. Probing the mechanism of insulin fibril formation with insulin mutants. *Biochemistry*. 40:8397–8409.

Nielsen, L., R. Khurana, A. Coats, S. Frokjaer, J. Brange, S. Vyas, V. N. Uversky, and A. L. Fink. 2001b. Effect of environmental factors on the kinetics of insulin fibril formation: elucidation of the molecular mechanism. *Biochemistry*. 40:6036–6046.

Nielsen, L., S. Frokjaer, J. F. Carpenter, and J. Brange. 2001c. Studies of the structure of insulin fibrils by Fourier transform infrared (FTIR) spectroscopy and electron microscopy. *J. Pharm. Sci*. 90:29–37.

Nettleton, E. J., P. Tito, M. Sunde, M. Bouchard, C. M. Dobson, and C. V. Robinson. 2000. Characterization of the oligomeric states of insulin in self-assembly and amyloid fibril formation by mass spectrometry. *Biophys. J*. 79:1053–1065.

Peretz, D., R. A. Williamson, G. Legname, Y. Matsunaga, J. Vergara, D. R. Burton, S. J. DeArmond, S. B. Prusiner, and M. R. Scott. 2002. A change in the conformation of prions accompanies the emergence of a new prion strain. *Neuron*. 34:921–932.

Perutz, M. F., J. T. Finch, J. Berriman, and A. Lesk. 2002. Amyloid fibers are water-filled nanotubes. *Proc. Natl. Acad. Sci. USA*. 99:5591–5595.

Rochet, J. C., and P. T. Lansbury. 2000. Amyloid fibrillogenesis: themes and variations. *Curr. Opin. Struct. Biol*. 10:60–68.

Rochet, J. C., T. F. Outeiro, K. A. Conway, T. T. Ding, M. J. Volles, H. A. Lashuel, R. M. Bieganski, S. L. Lindquist, and P. T. Lansbury. 2004. Interactions among α-synuclein, dopamine, and biomembranes: some clues for understanding neurodegeneration in Parkinson's disease. *J. Mol. Neurosci*. 23:23–34.

Serpell, L. C. 2000. Alzheimer's amyloid fibrils: structure and assembly. *Biochim. Biophys. Acta*. 1502:16–30.

Sipe, J. D., and A. S. Cohen. 2000. Review: history of the amyloid fibril. *J. Struct. Biol*. 130:88–98.

Sluzky, V., J. A. Tamada, A. M. Klibanov, and R. Langer. 1991. Kinetics of insulin aggregation in aqueous solutions upon agitation in the presence of hydrophobic surfaces. *Proc. Natl. Acad. Sci. USA*. 88:9377–9381.

Tanaka, M., P. Chien, N. Naber, R. Cooke, and J. S. Weissman. 2004. Conformational variations in an infectious protein determine prion strain differences. *Nature*. 428:323–328.

Westermark, P., C. Wernstedt, E. Wilander, D. W. Hayden, T. D. O'Brien, and K. H. Johnson. 1987. Amyloid fibrils in human insulinoma and islets of Langerhans of the diabetic cat are derived from a neuropeptide-like protein also present in normal islet cells. *Proc. Natl. Acad. Sci. USA*. 84:3881–3885.

Whittingham, J. L., D. J. Scott, K. Chance, A. Wilson, J. Finch, J. Brange, and G. G. Dodson. 2002. Insulin at pH 2: structural analysis of the conditions promoting insulin fibre formation. *J. Mol. Biol*. 318:479–490.